New Horizons in Time-Domain Astronomy
Proceedings IAU Symposium No. 285, 2011
R.E.M. Griffin, R.J. Hanisch & R. Seaman, eds.

doi:10.1017/S1743921312000646

Astrotomography

Keith Horne[1], Raymundo Baptista[2], Misty C. Bentz[3], and Danny Steeghs[4]

[1]SUPA Physics & Astronomy, University of St Andrews, St Andrews KY16 9SS, Scotland
email: kdh1(at)st-and.ac.uk

[2]Departmento de Fisica, Universidade Federal de Santa Catarina, Campus Trinidade, 88040-900 Florianopolis, SC, Brazil

[3]Department of Physics and Astronomy, Georgia State University, Atlanta, GA, 30303 USA

[4]Department of Physics, University of Warwick, Coventry CV4 7AL, UK

Abstract. Astrotomography refers to a suite of indirect imaging techniques that achieve micro-arcsecond angular resolution by measuring projections obtained from time-resolved spectroscopic observations. The projections arise from Doppler shifts, eclipses or time delays, combined with rotation of the star or binary system being imaged. At our workshop we reviewed and discussed state-of-the-art methods for imaging the surfaces and magnetic fields of rapidly rotating stars, the accretion flows in compact binary star systems and the broad emission-line regions in active galactic nuclei.

Keywords. accretion, accretion disks, black hole physics, methods: data analysis, techniques: high angular resolution, stars: binaries: eclipsing, galaxies: Seyfert

1. Astrotomography

Tomography reconstructs an image from measurements of its projections. It is widely used in geophysics to probe rock layers beneath the Earth's surface, and in medicine, where scanners project X-rays through a patient's body in various directions to obtain the projections needed to compute detailed diagnostic images of a patient's internal organs.

The Radon transform (Radon 1917) first demonstrated the equivalence of an image and its projections. Bracewell & Riddle (1967) pioneered the first practical applications, reconstructing maps of the radio sky using projections secured from lunar occultations or from fan beams of a linear antenna arrays. Modern interferometry—recovering images of the sky from measurements of projections of the image onto sine and cosine patterns with various wavelengths and position angles corresponding to the projected base-lines of pairs of telescopes—is closely related to tomography, where the projections are onto a basis of delta functions rather than sine and cosine functions.

In Doppler imaging of spotted stars (Vogt & Penrod 1983), Doppler shifts effectively project the visible hemisphere of a rotating star onto the observable radial-velocity profile of the star's spectral lines. The Least Squares Deconvolution (LSD) method (Donati & Collier Cameron 1997) collects information from thousands of weak spectral lines to form a mean velocity profile with a very high signal-to-noise ratio. Each starspot appears as a little bump in the line profile, rotating into view on the blue-shifted limb, crossing the face of the star and disappearing on the red-shifted limb. The spot's longitude determines the rotational phase at which the bump crosses the centre of the line profile; its latitude determines the range of phases and velocities spanned by the spot as it crosses.

In Zeeman-Doppler Imaging (Donati *et al.* 1997), high-resolution circular spectropolarimetry detects the polarised Zeeman components of rotating stellar magnetic fields.

The vertical, toroidal and poloidal field components have distinct polarisation signatures that march across the Doppler profile. From observations at a variety of rotation phases, the magnetic field vector is determined at each position on the surface of the rotating star.

Astrotomography methods for mapping accretion flows onto compact objects in binary systems and in active galactic nuclei were reviewed at our workshop by three expert practitioners, as reported below. In the discussion that followed we concluded that eclipse and Doppler mapping of accretion in binary systems is highly advanced observationally, with as yet untapped potential to validate models of accretion-disk atmospheres and chromospheres. In contrast, the echo mapping of accretion flows onto black holes in AGNs is currently limited by difficulties in obtaining suitable datasets, though there are prospects for improvement.

2. Eclipse Mapping of Accretion Disks

The light collected from Cataclysmic Variables (CVs) is the combination of emission from several distinct light sources, including the mass-donor star, the white dwarf (WD) at disk centre, the bright spot (BS) where infalling gas hits the outer disk rim, hotter inner regions plus the outer cooler regions of the accretion disk, and possibly vertically extended emission from a disk wind. Thus, interpreting and modelling the observed light from a CV is a degenerate problem that is usually plagued by the ambiguity associated with composite spectra. Nevertheless, for high-inclination systems ($i \geqslant 70^o$) the mass-donor star progressively covers different regions of the accretion disk, the WD and BS once per orbit, leading to eclipses. The shape of the eclipse has information about the surface brightness distribution of the occulted light sources. The maximum entropy eclipse mapping method (Horne 1985) is an inversion technique that assembles the information contained in the shape of the eclipse into a map of the accretion-disk surface brightness distribution plus the flux contribution of any uneclipsed source (e.g., the mass-donor star itself or a vertically-extended disk wind). It allows one to resolve structures spatially at angular scales of micro-arcseconds—well beyond the capabilities of present direct-imaging techniques.

2.1. *Principles and performance*

The mapping surface, know as the eclipse map, is defined as a grid of intensities centred on the WD. It can be either a flat grid in the orbital plane (standard eclipse mapping) or a conical surface with an outer cylinder (to account for a disk opening angle and for emission from the outer disk rim, 3-D eclipse mapping). The eclipse geometry is specified by the binary mass ratio q ($=M_2/M_1$, where M_2 and M_1 are the masses of the donor star and the WD, respectively) and the inclination i (see Horne 1985). Given the eclipse geometry, a model eclipse light curve can be calculated for any assumed brightness distribution in the eclipse map. A computer code then iteratively adjusts the intensities in the map (treated as independent parameters) to find the brightness distribution of the model light-curve which fits the eclipse lightcurve data within the uncertainties. The quality of the fit is checked by consistency statistics, usually the reduced χ^2. Because the one-dimensional light-curve data cannot fully constrain a two-dimensional map, additional freedom remains to optimize some map property. A maximum entropy procedure (e.g., Skilling & Bryan 1984) is used to select, among all possible solutions, the one that maximizes the entropy of the eclipse map with respect to a smooth default map, usually chosen as an axi-symmetric average of the eclipse map itself (see Baptista 2001).

https://doi.org/10.1017/S1743921312000646 Published online by Cambridge University Press

The quality of an eclipse map depends on the phase resolution and the signal-to-noise ratio (SNR) of the input light curve. Poor phase resolution degrades the spatial resolution of the eclipse map, while low SNR limits the ability to recover faint brightness sources. Good-quality maps can be obtained for $\Delta\phi < 0.005\,P_{\rm orb}$ and $SNR > 20$, while acceptable results can still be obtained for $\Delta\phi \leqslant 0.01\,P_{\rm orb}$ or $SNR \geqslant 8$. Examples of performance under extreme conditions are discussed by Baptista (2001).

2.2. *A range of applications*

Early applications of the technique were instrumental in showing that accretion disks in outbursting dwarf novæ (Horne & Cook 1985) and in nova-like variables (Rutten *et al.* 1992) closely follow the expected $T \propto R^{-3/4}$ dependence of temperature with radius for a steady-state opaque disk, and in inferring disk mass accretion rates. Eclipse mapping of time-resolved spectrophotometric data delivers the spectrum of the accretion disk at any position on its surface. For example, spectral mapping analysis of the nova-like variable UX UMa (Rutten *et al.* 1993; Baptista *et al.* 1998) shows that its inner accretion disk is characterized by a blue continuum filled with absorption bands and lines which cross over to emission with increasing disk radius, while at the same time the continuum emission becomes progressively fainter and redder, reflecting the radial temperature gradient. Physical conditions in the disk photosphere might be inferred by fitting those spectra properly with disk atmosphere models.

Time-resolved eclipse mapping can be used to trace the evolution of the disk surface-brightness distribution through a dwarf nova outburst cycle, and it allows critical tests of existing dwarf-nova outburst models. For example, time-lapse analysis of the dwarf nova EX Dra (Baptista & Catalán 2001) suggests that its outbursts are the response of a viscous disk to a burst of enhanced mass transfer from the donor star, in support of the mass-transfer instability model (Bath 1975). Eclipse mapping is also a valuable tool for revealing the existence of complex structures in accretion disks, such as tidally-induced spiral shocks in the dwarf nova IP Peg in outburst (Baptista *et al.* 2000) and the changing illumination pattern of disk regions produced by the fast spinning magnetosphere of the WD in the intermediate polar DQ Her (Saito & Baptista 2009).

Flickering mapping is the most recent frontier tackled with eclipse-mapping techniques. By combining a large ensemble of light curves one can measure the flickering amplitude as a function of orbital phase, and produce a map of the flickering sources from its eclipse shape (Baptista & Bortoletto 2004). Flickering mapping of the dwarf nova HT Cas in quiescence reveals a disk-related flickering component strongly concentrated near disk centre (Fig. 1).

Assuming that the disk flickering is caused by fluctuations in the energy dissipation rate induced by MHD turbulence in the disk's atmosphere (Geertsema & Achterberg 1992), one finds that the disk viscosity parameter is large in the inner disk and decreases with radius as $\alpha \propto R^{-2}$ (Baptista *et al.* 2011).

3. Doppler Tomography of Accretion Flows

Rapid optical variability and the presence of strong and broad emission lines are two key signatures of accretion onto compact objects in close binaries. Strong emission lines are produced by the hot accreting gas, and it was soon recognized that the line-profile shape is determined by bulk motion of the gas. Most commonly, the flow takes the form of an extended accretion disk reflecting the orbital angular momentum of the transferred gas. The observed line profile can thus be considered as a projection of the velocity distribution of the emitting gas in terms of its radial-velocity component. Time-series of

https://doi.org/10.1017/S1743921312000646 Published online by Cambridge University Press

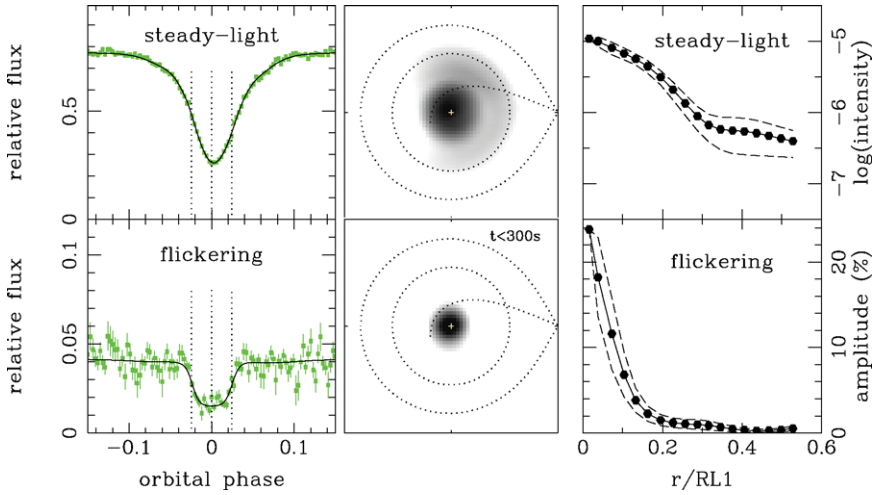

Figure 1. Flickering mapping of the dwarf nova HT Cas in quiescence. Left panels show data light curves (dots) and model light curves (solid lines). Middle panels display the corresponding eclipse maps in log intensity scale, while the right panels show the radial run of the steady-light intensity (top) and the relative amplitude of the flickering (bottom).

such profiles slice that emitting gas distribution as a function of the binary phase while the binary components orbit their common centre of mass. This presents a classic case of image reconstruction via a series of projections, which led to the development of Doppler tomography as a tool to image the emission-line distribution in compact binaries (Marsh & Horne 1988).

Although some explicit modelling of emission-line profiles can be done, asymmetries and complexities in the accretion flow make a model-driven reconstruction very difficult. However, thanks to the large dynamical velocities involved, detailed line-transfer effects that may set the local line-profile shape are overwhelmed by the bulk Doppler shifts. A model-independent reconstruction such as offered by Doppler tomography then presents a powerful and versatile tool. It has traditionally been employed for studying accreting white dwarfs in cataclysmic variables (Morales-Rueda 2004), but is applicable to a wide variety of systems including accreting neutron stars and black holes in X-ray binaries (Bassa *et al.* 2009), double degenerates (Roelofs *et al.* 2006) and Algols (Richards 2004). This variety also covers a range of flow geometries, from the more traditional accretion-disk dominated flow to streams (Kafka *et al.* 2010), propellers (Welsh *et al.* 1998) and magnetically controlled flows (Schwope *et al.* 2004).

The original version employed a regularised fitting procedure driven by maximum entropy constraints analogous to eclipse mapping (see above). Filtered back-projections offer a more straightforward implementation, but with the improvement of computational power the entropy-regularised implementation is the more popular choice. It gives some notable advantages, including having an explicit goodness of fit statistic driving the reconstructions, dealing with data imperfections and gaps, handling line blends, and being easily extendible (Marsh 2001; Steeghs 2003). The required input data are the emission-line flux resolved in both velocity and time. The spectral resolution effectively sets the velocity resolution of the reconstructed tomogram in the radial direction, while the time/phase resolution sets the azimuthal resolution. When planning Doppler tomography observations, a sensible compromise between spectral resolution and exposure time needs to be made that still offers an adequate S/N.

https://doi.org/10.1017/S1743921312000646 Published online by Cambridge University Press

The central concept in Doppler tomography is the realisation that an emission-line source location can be characterised not just by its location in spatial coordinates but also in terms of its velocity vectors. The vector encodes both the size and orientation of the source velocity, and is sufficient to establish the projected radial-velocity components of such a source as a function of time. The observed line profile at a given binary phase is then a simple summation of all emission line sources as specified by their individual velocity vectors. The image we then seek to reconstruct is an intensity map in velocity coordinates. By working in velocity space, the problem is a straight de-projection from the data. We do not need to assume the velocity field of the flow that would be necessary to convert between spatial and velocity coordinates. The downside of this approach is that the reconstructed images are in a somewhat unfamiliar coordinate frame. However, it is recommended that one maps models to the velocity frame for direct comparison with tomograms in velocity space, as opposed to reconstructing the data in spatial coordinates (Steeghs & Stehle 1999).

Doppler tomography is now a widely-used tool that has supported a large volume of published studies which employ Doppler tomograms in a variety of binaries. When S/N is limited, one is often constrained to using only the strongest lines; however, it is increasingly clear that the Balmer lines are by no means the best lines to map despite their relatively large strengths. For example, van Spaandonk *et al.* (2010) highlight the sensitivity of the Ca II triplet both in terms of providing sharper images of the accretion disk and also in revealing emission components from faint donor stars.

Beyond mapping the accretion-flow dynamics, Doppler tomography can also be used to constrain fundamental binary parameters. Simple dynamical models such as the trajectory of the in-falling ballistic stream, or the solid-body rotation of the mass donor star, are often sufficient to constrain the binary mass ratio and the orbital velocities of the binary components directly. Such models can then be compared with the observed locations of stream-disk interactions or donor star emission components (Steeghs & Casares 2002; see also Fig. 2).

Larger telescopes and more efficient detectors and spectrographs now permit Doppler tomography of rather faint objects. At the same time, the application of higher S/N and spectral resolution to systems previously studied offers a step change in tomogram quality. It is unfortunate that we are often not in a position to model the observed tomograms in great detail. Emission-line formation processes in these accreting systems are complex, and sufficiently realistic models that predict emission-line profiles at the level of detail offered by many data sets are not really available. That also prevents us from exploiting quantitatively, beyond broad trends, the information contained in mapping multiple emission lines within the same system.

Ample opportunities remain to develop the technique further. They include considering full 3-D velocities, exploiting the direct constraints on the spatial location of a source during eclipses by combining Doppler tomography and eclipse mapping, and reconstructing physical-parameter maps as opposed to single emission-line distribution maps.

4. Reverberation Mapping of AGN Broad-Line Regions

Active galactic nuclei (AGNs) are some of the most energetic objects in the universe. The emission from photoionized gas near a supermassive black hole can rival that of all the stars in the host galaxy, yet it is emitted from a region comparable in size to our Solar System (1000 AU, or $\sim$0.01 pc). Although such regions are spatially unresolvable in even the most nearby AGNs, studies of the gas in the broad-line region (BLR: the region of photoionized gas from which the broad emission lines in AGN spectra are

https://doi.org/10.1017/S1743921312000646 Published online by Cambridge University Press

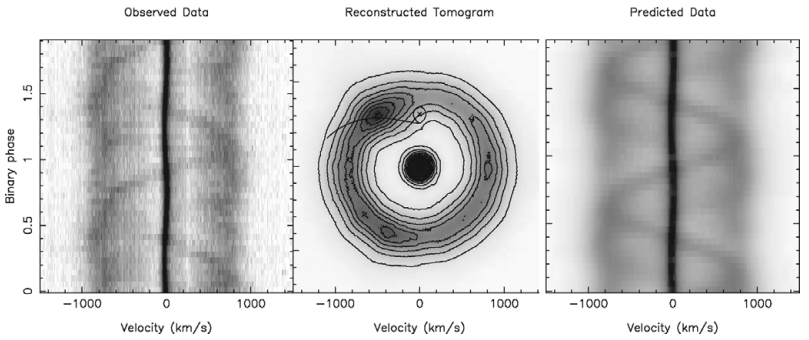

Figure 2. Doppler tomogram showing the distribution of He I emission in the double degenerate binary GP Com, compared to the observed input data and the reconstructed data. We see the near-circular accretion disk with a bright spot in the location where the in-falling gas stream hits the outer disk. In GP Com the accreting white dwarf is also an emission-line source visible near the center of mass. By fitting the locations of such features one can constrain binary parameters directly.

emitted) are critical to our understanding of galaxy and black-hole growth and co-evolution throughout cosmic time.

Black-hole masses for active galaxies are most often determined through the technique of reverberation mapping (Blandford & McKee 1982; Peterson 1993). The rarity of AGNs means that they are generally found at distances that are prohibitive for dynamical modelling (which is limited by spatial resolution); however, reverberation mapping replaces spatial resolution with time resolution. By monitoring the AGN's continuum flux (which is produced near the black hole, probably in the accretion disk) and the time-delayed response of the broad emission lines to changes in that continuum flux, it is possible to deduce the average radius of the BLR. Combining that radius with the velocity-broadened width of the emission line through the virial theorem provides a measure of the black-hole mass, though with a scaling factor that depends on the geometry and kinematics of the BLR gas. To date, some 50 black-hole masses have been determined in this way (Peterson *et al.* 2004; Bentz *et al.* 2009) and provide the basis for *all* black-hole mass determinations in AGNs at cosmological distances.

The limiting factor in the accuracy of these black-hole masses is the scaling factor, f. The current practice is to assume that the $M_{\rm BH} - \sigma_\star$ relationship for quiescent galaxies with dynamical black-hole masses is the same as the $M_{\rm BH} - \sigma_\star$ relationship for active galaxies with reverberation masses. The scaling factor is then taken to be the average multiplicative factor required to bring the two relationships into agreement, and has been found to be $\langle f \rangle \sim 5$ (Onken *et al.* 2004; Woo *et al.* 2010). However, reverberation mapping has the potential to map directly the response of the gas in the BLR as a function of time delay and velocity, thereby providing stringent constraints on the geometry and kinematics of the BLR gas. With such constraints, f could be determined on an individual basis rather than an average basis, and the black-hole mass would be constrained directly without relying on the sample of objects with masses determined by dynamical modelling.

The challenge has been to acquire data of the quality necessary to control observational systematics and recover the full response of the broad emission lines. However, recent spectroscopic monitoring campaigns have been achieving high sampling cadences and high S/N spectra over long durations, and are now allowing us to reach the level of observational accuracy that is necessary to see differences in the mean response as a function of velocity across the line profile (Bentz *et al.* 2009; Denney *et al.* 2009). A

https://doi.org/10.1017/S1743921312000646 Published online by Cambridge University Press

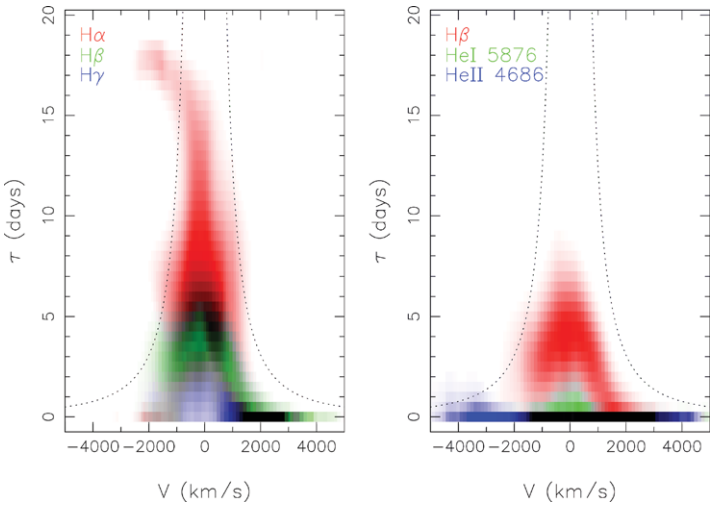

Figure 3. Optical broad emission-line response as a function of time delay and velocity for the $z = 0.02$ AGN Arp 151. From Bentz *et al.* (2010).

substantial effort is currently being invested in mapping the full BLR gas response, and is meeting with some success.

Fig. 3 shows the recovered response of five broad emission lines in the spectrum of Arp 151 as a function of velocity and time delay (from Bentz *et al.* 2010). For comparison, Fig. 4 shows the expected response for three different kinematic models of an AGN BLR. The higher ionization lines in Arp 151 are seen to vary on much shorter timescales than the lower ionization lines, as has been observed for many AGNs, indicating ionization stratification in the BLR. The Balmer-line response is somewhat consistent with emission arising from a flattened-disk geometry; however, the response is distinctly asymmetric, with a strong response at short time delays in the red-shifted wing of the emission lines and with much longer time delays in the blue wing. This asymmetry in the line response may arise from a strong infall component in the BLR of Arp 151, or it may arise from a disk asymmetry such as a warp or hotspot.

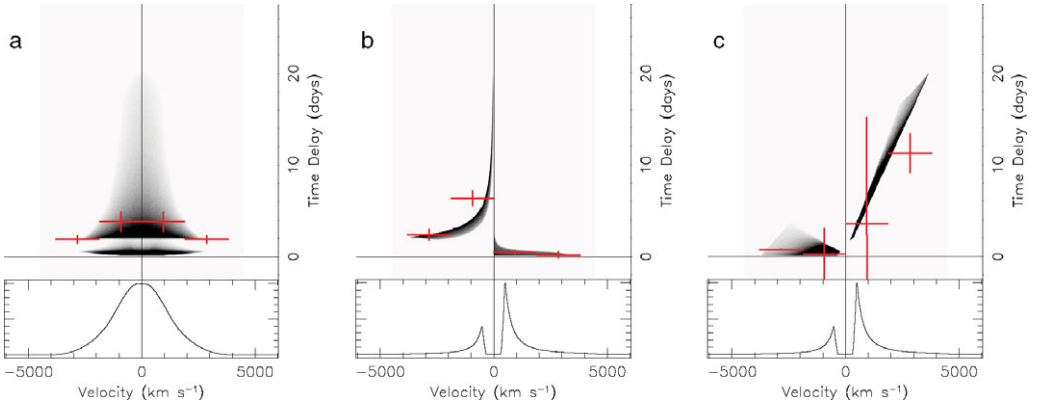

Figure 4. Models of the broad line response as a function of velocity and time delay for (a) a Keplerian disk, (b) an infalling BLR and (c) a constantly-accelerated outflow. From Bentz *et al.* (2009).

https://doi.org/10.1017/S1743921312000646 Published online by Cambridge University Press

It is vital that our observations and analysis continue to improve, because reverberation mapping has the potential to answer fundamental questions about the fuelling of AGNs, to provide a solid basis upon which to determine black-hole masses at cosmological distances, and to increase our knowledge of the growth and co-evolution of galaxies and black holes throughout cosmic history.

References

Baptista, R., *et al.* 1998, *MNRAS*, 298, 1079

Baptista, R., Harlaftis, E. T., & Steeghs, D. 2000, *MNRAS*, 314, 727

Baptista R. 2001, in: H.M.J.Boffin, D.Steeghs & J.Cuypers (eds.), *Astrotomography: Indirect Imaging Methods in Observational Astronomy* (Berlin: Springer-Verlag), p. 307

Baptista, R. & Catalán, M. S. 2001, *MNRAS,* 324, 599

Baptista, R. & Bortoletto, A. 2004, *AJ*, 128, 411

Baptista, R., *et al.* 2011, Proceedings of *Physics of Accreting Compact Binaries*, (Universal Academic Press Inc.), in press. (arXiv 1105.1382)

Bassa, C. G., Jonker, P. G., & Steeghs, D. 2009, *MNRAS*, 399, 2055

Bath, G. T. 1975, *MNRAS*, 171, 311

Bentz, M. C., *et al.* 2009, *ApJ*, 705, 419

Bentz, M. C., *et al.* 2010, *ApJ*, 720, L46

Blandford, R. D. & McKee, C. F. 1982, *ApJ*, 255, 419

Bracewell, R. N. & Riddle, A. C. 1967, *ApJ*, 150, 427

Denney, K. D., *et al.* 2009, *ApJ*, 704, L80

Donati, J.-F. & Collier Cameron, A. 1997, *MNRAS*, 291, 1

Donati, J.-F., Semel, M., Carter, B. D., Rees, D. E., & Collier Cameron, A. 1997, *MNRAS*, 291, 658

Geertsema, G. T. & Achterberg, A. 1992, *A&A*, 255, 427

Horne, K. 1985, *MNRAS*, 213, 129

Horne, K. & Cook, M. C. 1985, *MNRAS*, 214, 307

Kafka S., Tappert C., Honeycutt, R. K. 2010, *MNRAS*, 403, 755

Marsh, T. R. 2001, in: H.M.J.Boffin, D.Steeghs & J.Cuypers (eds.), *Astrotomography: Indirect Imaging Methods in Observational Astronomy* (Berlin: Springer-Verlag), p. 1

Marsh, T. R. & Horne, K. 1988, *MNRAS*, 235, 269

Moralez-Rueda L. 2004, *AN*, 325, 193

Onken, C. A., *et al.* 2004, *ApJ*, 615, 645

Peterson, B. M. 1993, *PASP*, 104, 247

Peterson, B. M., *et al.* 2004, *ApJ*, 613, 682

Radon, J. 1917, *Ber. Sächs. Akad. Wiss. Leipzig, Math. Phys*, 69, 262

Richards, M. T. 2004, *AN*, 325, 229

Roelofs, G., Groot, P., Marsh, T. R., Steeghs, D., & Nelemans, G. 2006, *MNRAS*, 365, 1109

Rutten, R. G. M., van Paradijs, J., & Tinbergen, J. 1992, *A&A*, 260, 213

Rutten, R. G. M., Dhillon, V. S., Horne, K., Kuulkers, E., & van Paradijs, J. 1993, *Nature*, 362, 518

Saito, R. K. & Baptista, R. 2009, *ApJ*, 693, L16

Schwope, A., Staude, A., Vogel, J., & Schwarz, R. 2004, *AN*, 325, 197

Skilling, J. & Bryan, R. K. 1984, *MNRAS*, 211, 111

Steeghs, D. 2003, *MNRAS*, 344, 448

Steeghs, D. & Casares, J. 2002, *ApJ*, 568, 273

Steeghs, D. & Stehle, R. 1999, *MNRAS*, 307, 99

van Spaandonk, L., Steeghs, D., Marsh, T. R., & Torres, M. A. P. 2010, *MNRAS*, 401, 1857

Vogt, S. S. & Penrod, G. D. 1983, *PASP*, 95, 565

Welsh, W. F., Horne, K., & Gomer, R. 1998, *MNRAS*, 298, 285

Woo, J. H., *et al.* 2010, *ApJ*, 716, 269